Assessing the thermal conductivity of amorphous SiN by approach-to-equilibrium molecular dynamics

Achille Lambrecht, Guido Ori, Carlo Massobrio, Mauro Boero, Évelyne Martin

▶ **To cite this version:**

Achille Lambrecht, Guido Ori, Carlo Massobrio, Mauro Boero, Évelyne Martin. Assessing the thermal conductivity of amorphous SiN by approach-to-equilibrium molecular dynamics. The Journal of Chemical Physics, 2024, 160 (9), pp.094505. 10.1063/5.0193566 . hal-04490310

HAL Id: hal-04490310
https://hal.science/hal-04490310v1

Submitted on 5 Mar 2024

HAL is a multi-disciplinary open access archive for the deposit and dissemination of scientific research documents, whether they are published or not. The documents may come from teaching and research institutions in France or abroad, or from public or private research centers.

L'archive ouverte pluridisciplinaire **HAL**, est destinée au dépôt et à la diffusion de documents scientifiques de niveau recherche, publiés ou non, émanant des établissements d'enseignement et de recherche français ou étrangers, des laboratoires publics ou privés.

ACCEPTED MANUSCRIPT
The Journal of Chemical Physics
AIP Publishing
This is the author's peer reviewed, accepted manuscript. However, the online version of record will be different from this version once it has been copyedited and typeset.
PLEASE CITE THIS ARTICLE AS DOI: 10.1063/5.0193566

Assessing the thermal conductivity of amorphous SiN by approach-to-equilibrium molecular dynamics

Achille Lambrecht
Université de Strasbourg, CNRS, Institut de Physique et Chimie des Matériaux de Strasbourg, UMR 7504, Strasbourg F-67034, France and Université de Strasbourg, CNRS, Laboratoire ICube, UMR 7357, F-67037 Strasbourg, France

Guido Ori and Carlo Massobrio
Université de Strasbourg, CNRS, Institut de Physique et Chimie des Matériaux de Strasbourg, UMR 7504, Strasbourg F-67034, France

Mauro Boero
Université de Strasbourg, CNRS, Institut de Physique et Chimie des Matériaux de Strasbourg, UMR 7504, Strasbourg F-67034, France and Institute of Materials and Systems for Sustainability, Nagoya University, Nagoya 464-8603. Japan

Evelyne Martin*
Université de Strasbourg, CNRS, Laboratoire ICube, UMR 7357, F-67037 Strasbourg, France
(ADynMat consortium)†
(Dated: February 6, 2024)

First principles molecular dynamics (FPMD) combined with the approach-to-equilibrium molecular dynamics (AEMD) methodology is employed to calculate the thermal conductivity of non-stoichiometric amorphous SiN (*a*-SiN). This is achieved by implementing thermal transients in five distinct models of different sizes along the direction of the heat transport. Such models have identical structural features and are representative of the same material, thereby allowing for a reliable analysis of thermal conductivity trends as a function of the relevant cell dimension. In line with the known physical law of heat propagation at short scale, the thermal conductivity increases with size in the direction of heat transport. The observed behavior is rationalized accounting for previous results on crystalline and amorphous materials, thus providing a unified description holding for a large class of materials and spanning a wide range of heat propagation lengths.

I. INTRODUCTION

Amorphous materials are commonly utilised in electronic and photonic devices owing to their intrinsic properties and a production process that is often simpler compared to regular crystal growth. The ability of amorphous materials to conduct heat is of paramount importance in devices driven by Joule heating, such as phase-change memories [1] or reconfigurable metasurfaces [2], and when heat is generated under operation, as in solid state batteries [3]. Despite recent advances [4–7], precise understanding of thermal transport in amorphous materials is considerably less developed compared to their crystalline counterparts.

We have recently combined the approach-to-equilibrium molecular dynamics (AEMD)[8] and the description of interatomic forces within first-principles molecular dynamics (FPMD) to extract the thermal conductivity from the simulation of a thermal transient [9]. In the present work, we have selected amorphous SiN (*a*-SiN, Si_xN_y with $x = y$) as a representative non-stoichiometric silicon nitride system. This choice stems from its wide use in microelectronics and micromechanics manufacturing [10], due in particular to a lower level of internal stress compared to the stoichiometric compound Si_3N_4 [11]. Furthermore, the values of thermal conductivity reported in the literature for bulk *a*-SiN are unexpectedly high for an amorphous material (around 3 W K^{-1} m^{-1}). In a recent work [12], we generated and characterized the atomic structure of *a*-SiN at finite temperature using FPMD. The resulting model provides a highly representative and accurate description of *a*-SiN.

In this paper, the same protocol is followed (see Section IIA) to obtain three additional models of *a*-SiN. We obtain a collection of five data points from which, by applying the AEMD methodology, the relationship between size in the heat propagation direction and thermal conductivity can be inferred. We go beyond the standard cases of amorphous silicon and amorphous silica to focus on a material differing from those considered so far, namely chalcogenides and oxides. This allows enhancing knowledge of the thermal properties of disordered materials and contribute to the ongoing discussion on heat transfer, by providing accurate quantitative data that cannot be obtained through measurements. In addition, we are able to quantify the evolution at small scales of thermal conductivity in a material of great experimental interest, this information being crucial to prevent blind

* evelyne.martin@unistra.fr
† https://www.adynmat.cnrs.fr

ACCEPTED MANUSCRIPT
The Journal of Chemical Physics
AIP Publishing
This is the author's peer reviewed, accepted manuscript. However, the online version of record will be different from this version once it has been copyedited and typeset.
PLEASE CITE THIS ARTICLE AS DOI: 10.1063/5.0193566

optimization of technological devices.

To emphasize the link between the determination of the structural properties and the calculations of thermal conductivity, the AEMD methodology is recalled in Section IIB. The purpose is to explain in detail how to cope with the lack of adiabaticity inherent in some of the Car-Parrinello calculations in order to make them compatible with the AEMD scheme (passivation of dangling bonds). Section III is devoted to the results for the structural properties (IIIA) and the thermal conductivity (IIIB). A thorough discussion of the behavior of thermal conductivity in amorphous nanosystems, together with a rational devoted to their physical origins, is presented in Section IV. Considerations relative to the different predictive power of AEMD when compared to phenomenological models are also included. Conclusions are drawn in Section V.

II. METHODOLOGY OF CALCULATION

A. Atomic models and implementation of first-principles molecular dynamics

Atomic models of non-stoichiometric a-SiN were generated by fixing the cross section of the simulation cell and by varying the length L_z along the z direction, where heat transport processes will occur. The models realized in our previous [12] and present calculations are shown in Fig. 1. All the simulation cells are orthorombic with sides equal to $L_x = 10.0$ Å and $L_y = 20.0$ Å in the x and y directions, respectively. Periodic boundary conditions are applied in the three directions. For each system and total volume, the number of atoms N corresponds to the value of the experimental density (2.98 g cm^{-3})[13] with an identical ratio between the number of Si atoms and the number of N atoms as summarized in Table I, where the total number of atoms N and the corresponding L_z for the five models are reported.

N	252	340	680	1020	1360
L_z (Å)	15	20	40	60	80

TABLE I. Number of atoms N and cell length L_z along the heat transport direction for the five systems created in Ref. [12] and in the present work to obtain the thermal conductivity of a-SiN.

To perform first-principles molecular dynamics (FPMD) calculations, we use both the Car-Parrinello [14] and the Born-Oppenheimer [15] methods, within the density functional theory (DFT) framework. For the exchange and correlation interactions, we selected the functionals proposed by Becke [16] and Lee, Yang and Parr [17] (BLYP), respectively. Valence-core interactions are described by norm-conserving pseudopotentials in the numerical version of Troullier and Martins [18]. Valence electrons are explicitly treated and their wavefunctions expressed on a plane-wave basis set with a cutoff of 70 Ry. The sampling of the Brillouin zone is limited to the Γ point. For the Car-Parrinello scheme, the mass of the fictitious electronic degrees of freedom was set to 800 a.u. and the time step for the numerical integration of the equations of motion was set to 5 a.u. (0.12 fs), ensuring optimal conservation of the constants of motion. The ionic temperature was controlled with a Nosé-Hoover [19–22] thermostat chain [23]. An additional thermostat is applied to the fictitious electronic kinetic energy as pioneered by Blöchl and Parrinello [24]. When resorting to the Born-Oppenheimer method, the time step is increased to 100 a.u. (2.4 fs). The electronic structure is then optimized at each step of the ionic dynamics by applying the following convergence criterion on the total energy. Whenever the ground state total energy reaches an accuracy with a residual error lower than 10^{-6} a. u., the convergence is retained as achieved. For a critical review on the combined use of Car-Parrinello and Born-Oppenheimer methods in a-SiN, we refer to Ref. [12]. All simulations were performed with the CPMD package [25].

At the beginning, initial atomic coordinates are taken from previously generated sets for disordered systems [26–28]. Then, a thermal cycle is implemented by increasing the temperature in a step-wise fashion within the canonical NVT ensemble [19–22]. This allows loosing memory of the initial configuration and ensures substantial diffusion, a necessary prerequisite to the realization of a reliable amorphous network. As customarily done when producing amorphous systems, subsequent quench to room temperature drives the system into a configuration that can be taken as frozen ("configurationally arrested") even on the most extended time scales accessible to molecular dynamics endeavors. In the search for a highly diffusive behavior, we had to reach temperatures higher than the melting temperature located at T= 2500 K. With this constraint in mind, atomic trajectories along the thermal cycle are produced up to T= 1500 K by the Car-Parrinello version of FPMD. For higher temperatures, since a large amount of dangling bonds is produced with a related substantial reduction of the gap in the electronic density of states (EDOS), the method suffers from the known shortcomings resulting in a loss of adiabaticity [12, 29]. To overcome this difficulty, at higher temperature we switched to the Born-Oppenheimer scheme [30] along with a re-optimization of the eigenfunctions at each step. The computational workload to produce the thermal cycles reflects the sizes of the five models. For the system containing N= 680 atoms, the thermal cycle was similar to the one used in Ref. [12] to produce the two smaller systems (N = 252 and 340). A total simulation time of 300 ps encompassed temperature steps of T = 300, 1000, 1500, 2000 and 2500 K for the heating process, followed in the case of N= 1020 and N= 1360, by an additional step of a few ps at T = 3000 K. The subsequent cooling process featured temperatures T = 2000,

ACCEPTED MANUSCRIPT
The Journal of Chemical Physics
AIP Publishing
This is the author's peer reviewed, accepted manuscript. However, the online version of record will be different from this version once it has been copyedited and typeset.
PLEASE CITE THIS ARTICLE AS DOI: 10.1063/5.0193566

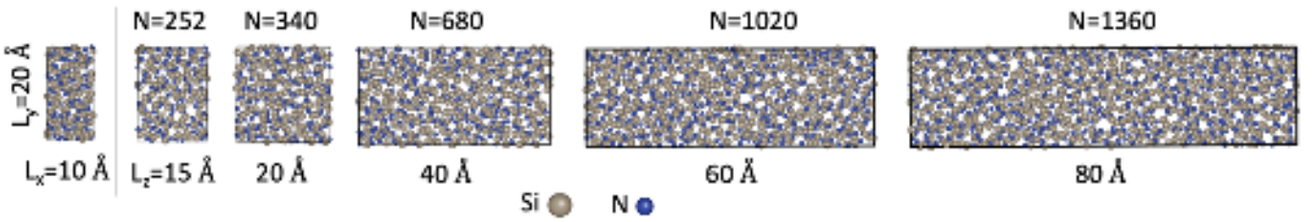

FIG. 1. Atomic models of amorphous SiN. The smaller models containing $N = 252$ and 340 atoms are from Ref. [12]. The five models have the same cross section (L_x =10Å×L_y=20Å), whereas their length L_z along the z axis is comprised between 15 and 80 Å.

1500, 1000, 500 K and a final equilibrium run at $T =$ 300 K. For the larger sizes, because of the non-negligible computational workload, the total simulation time for the thermal cycle was reduced to 100 ps for $N = 1020$ and to 70 ps for $N = 1360$, by adopting the same sequence of temperature steps on correspondingly shorter trajectories.

B. Thermal conductivity: the AEMD method

The thermal conductivity of a-SiN was calculated by resorting to the AEMD methodology [8, 31–33]. In this approach, we exploit the thermal transient regime described by the heat equation, characterized by the following relationship between the transient decay time τ and the thermal conductivity κ

$$\kappa = \frac{L^2}{4\pi^2}\frac{C.\rho}{\tau}. \quad (1)$$

Eq. 1 holds provided the heat transfer occurs in one direction between hot and cold blocks alternating periodically, the periodicity being ensured by the use of periodic boundary conditions. In Eq. 1, C is the heat capacity extracted from the variation of the total energy as a function of the temperature. Total energies and temperatures were collected at different steps of the thermal cycle. We found a value slightly departing from the Dulong and Petit formula, namely $C = 3\gamma N k_B$ with $\gamma = 1.12$ for a-SiN. The transient time τ is obtained by setting each half of the cell along the z direction at different temperatures (phase 1 of the AEMD methodology). In this work, T_1 = 200 K and T_2 = 400 K, i.e. ΔT_0 = 200 K. Values of τ were found insensitive to ΔT_0 within the [50-300K] temperature range [32, 34], the statistical error being reduced for $\Delta T_0 > 150$ K. Then, the systems are left to approach the equilibrium by removing the thermostats acting on the two blocks (phase 2). Therefore, the thermostats are used during phase 1 to keep two adjacent parts of the system at different temperatures, while during phase 2 all thermostats are removed. This last condition is crucial to ensure the reliability of the AEMD approach in reproducing the correct relaxation to a uniform distribution of temperature throughout the entire system. It should be kept in mind that phase 2 features a temperature transient characterized by a very rapid increase (decay) from T_1 (T_2) to the target T (300 K in our case). For this reason, within phase 2, T_1 and T_2 are by no means equilibrium temperatures, thereby ruling out any undesirable effect due to a dependence on T of the thermal conductivity [35, 36].

Combining AEMD with the Car-Parrinello approach can be non trivial in practice. This occurs when the absence of a finite band gap in the electronic density of states results in an undesirable energy transfer from the ionic to the electronic degrees of freedom. Such non adiabatic process, causing the electronic degrees of freedom to move away from their ground state, is incompatible with phase 2 of AEMD. Since we did encounter such shortcomings for some of our systems, it is necessary to describe how we handled them in order to implement AEMD in connection with the Car-Parrinello scheme. The upper panel of Fig. 2 shows, for the case N=1020, under which conditions we were in gap-closing conditions jeopardizing the Car-Parrinello method. This phenomenon arises as a consequence of the shorter duration of the thermal cycle for the larger systems preventing a full reorganization of the network and the annealing of a few defects. We have also to recall that, due to our selection of an equal amount of Si and N atoms, a certain amount of Si–Si homopolar bonds appeared in our amorphous models. This induces in the EDOS the presence of a Si-like gap (about 1.1 eV) which is much smaller than the wide band gap of Si_3N_4 (about 4.7 eV). To get a deeper insight into this problem, we calculated the participation ratio of the states in proximity of the Fermi level, and identified high values typical of localized states. After finding two atoms exhibiting a dangling bond, we added hydrogen atoms at the position of the corresponding Wannier centers [37] to passivate these dangling bonds. Then, relaxation followed to allow for structural rearrangement. The lower panel of Fig. 2 shows the EDOS after the addition of these extra H atoms and subsequent relaxation. A finite band gap is recovered, thereby ensuring that the Car-Parrinello dynamics can be applied during phase 2 of AEMD and the adiabatic condition is preserved. Further check of the pair correlation functions indicates that the inclusion of two H atoms did not impact the overall atomic structure. We wish to stress also that the presence of hydrogen in

ACCEPTED MANUSCRIPT
The Journal of Chemical Physics
AIP Publishing
This is the author's peer reviewed, accepted manuscript. However, the online version of record will be different from this version once it has been copyedited and typeset.
PLEASE CITE THIS ARTICLE AS DOI: 10.1063/5.0193566

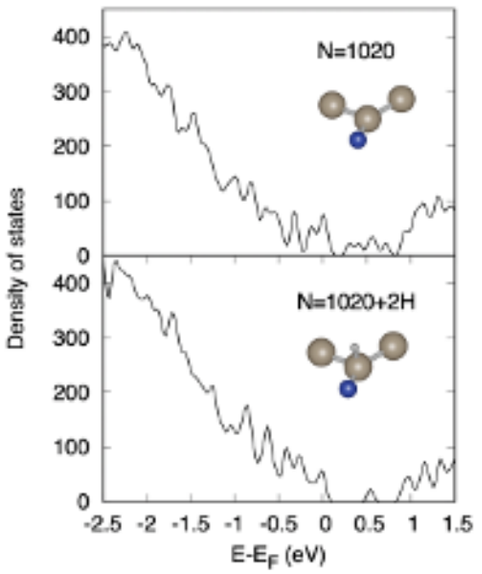

FIG. 2. Electronic density of states (EDOS) around the Fermi level for a-SiN containing N=1020 atoms (upper panel) plus two H atoms (lower panel). In inset, atomic configuration before and after adding an H atom to passivate a dangling bond.

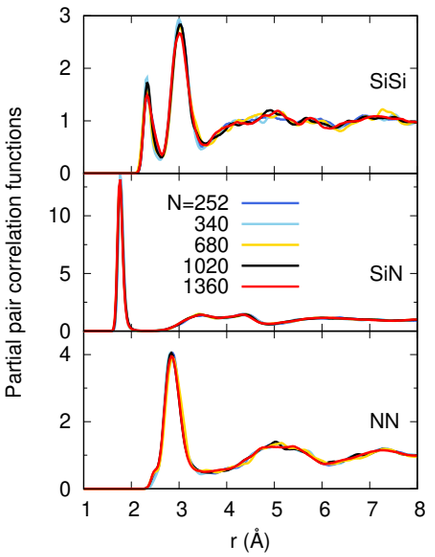

FIG. 3. Partial pair correlation functions of the atomic models of a-SiN containing up to N = 1360 atoms.

a-SiN has a realistic character since, due to preparation techniques and conditions [10], concentrations of hydrogen as high as 15 at.% can be recorded experimentally [13]. These are well above the value of 0.2 at.% corresponding to the addition of two hydrogen atoms in a cell of 1020 atoms.

III. RESULTS

A. Structural properties

We were able to obtain five models of a-SiN characterized by very similar structural arrangements in terms of partial pair correlation functions (PCFs), as shown in Fig. 3.

We report in Table II the nearest neighbor distances, corresponding to the first maximum of each PCF, and the coordination numbers calculated by integrating each PCF up to their first minimum. Note that for the Si–N case the profile does not feature any significant change in the range 2.02 Å- 2.65 Å. In this case the value given for the nearest neighbor distance is taken to be at the center of the interval given above. The peak positions and the coordination numbers reproduce those reported in Ref. [12], indicating a consistency of the present results with the former ones. We recall that N atoms were found three-fold coordinated exclusively to Si atoms, in a way similar to what occurs in the stoichiometric compound Si_3N_4[13]. Furthermore, Si atoms turned out to be four-fold coordinated by accommodating Si extra atoms via homopolar Si–Si bonds. We found that Si–Si nearest neighbor distances are larger than the Si–N ones accounting for the peak at 2.33 Å in the Si–Si correlation function. This value is consistent with the distances in pure Si structures, both crystalline and amorphous, where Si–Si bond distances range between 2.32 and 2.36 Å.

TABLE II. Nearest neighbor distances (d_{NN}) between Si–N, Si–Si and N–N atoms and coordination numbers (CN). CN were computed by integrating each PCF up to their first minimum. Results are given for each model and averaged on the five models produced for amorphous silicon nitride.

		Si–N	Si–Si		N–N	
	N	1st	1st	2nd	1st	2nd
d_{NN}(Å)	252	1.76	2.33	3.12	–	2.87
	340	1.76	2.33	3.01	–	2.81
	680	1.76	2.33	3.04	–	2.84
	1020	1.76	2.33	3.01	–	2.87
	1360	1.76	2.33	3.01	–	2.84
	Av.	1.76	2.33	3.04±0.02	–	2.84±0.01
CN	252	3.02	1.15	–	–	–
	340	3.02	1.12	–	–	–
	680	3.03	1.20	–	–	–
	1020	3.03	1.18	–	–	–
	1360	3.03	1.23	–	–	–
	Av.	3.02±0.01	1.18±0.01	–	–	–

B. Thermal conductivity

Before focusing on the results obtained for the thermal conductivity of SiN, it is of interest to consider some

ACCEPTED MANUSCRIPT
The Journal of Chemical Physics
AIP Publishing
This is the author's peer reviewed, accepted manuscript. However, the online version of record will be different from this version once it has been copyedited and typeset.
PLEASE CITE THIS ARTICLE AS DOI: 10.1063/5.0193566

typical behavior observed for the temperature of the system as a result of the application of phase 1 and phase 2 of AEMD recalled in Section II B. When averaging over phase 2, one obtains a temperature profile that takes a sinusoidal shape (green curve in Fig. 4), as it stems from the Fourier equation for the transitory regime of heat transport [8, 33]. Fig. 5 shows the temperature of the hot

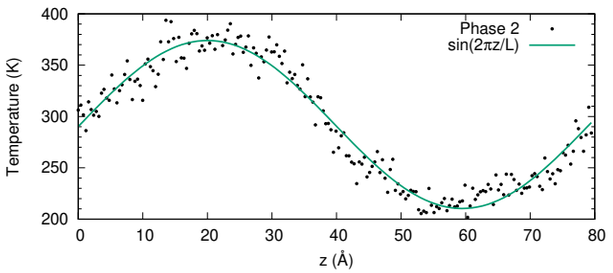

FIG. 4. Temperature averaged over the whole phase 2 (dots). Note that the profile is sinusoidal (green line, fit to the data). This specific result refers to the system with N=1360.

and cold blocks during a typical sequence of phases 1 and 2 aimed at obtaining the average of the thermal conductivity as well as an estimate of the error bar by selecting different starting point for the transition from phase 1 to phase 2. The transient times are determined by fitting

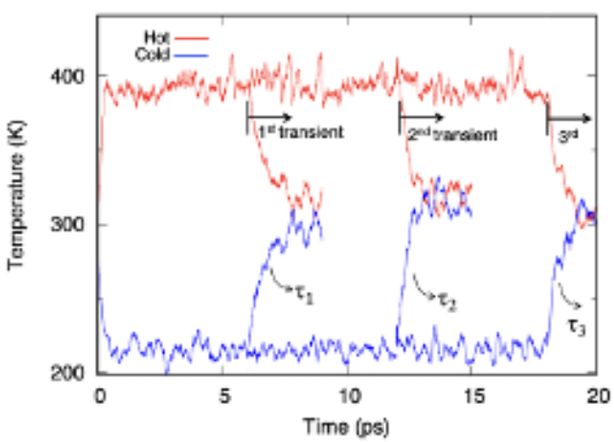

FIG. 5. Temperature evolution in the hot (red lines) and cold (blue lines) blocks during a series of phases 1 (constant temperature) and phases 2 (transient). Three transient times τ_1, τ_2 and τ_3 are extracted by fitting the transient decay to an exponential function. This specific result refers to the system with N=340.

the temperature difference between the two blocks to an exponential decay during phase 2. Each temperature is the average over the corresponding block.

Results for the thermal conductivity are shown in Fig. 6. We have reported values obtained by the sequence of distinct phases 2, with the average and error bar plotted in a different color for the sake of clarity. An

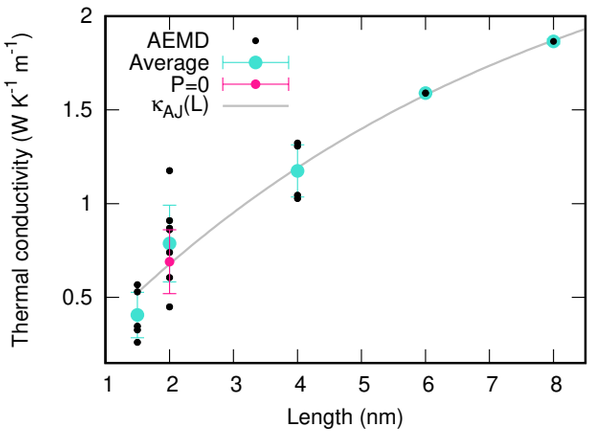

FIG. 6. Thermal conductivity of a-SiN as a function of the length of the simulation cell/period of thermal signal. The black dots refer to the AEMD results. Their average is highlighted in turquoise with their associated error bars. The pink dot was obtained after an NPT simulation at $P = 0$. The grey curve is the fit obtained according to Eq. 2.

additional point was obtained by including a constant pressure NPT result before starting the AEMD phases. The target pressure was set to 0 GPa with an error bar of 0.2 GPa. As shown in Fig. 6, the corresponding change (1.3%) in the cell dimensions does not impact the thermal conductivity, in line with the measurement of Ftouni et al [11]. Coming back to the series of thermal conductivity results, we remark that κ increases in the range between 1.5 and 8 nm. At 8 nm, κ is equal to 1.86 W K^{-1} m^{-1}.

The thermal conductivity of a-SiN has been targeted by several former publications for a variety of deposition method, stoichiometry, density, and H-content; for a review see Ref. [38]. For a stoichiometry between 1 and 1.1 and a density in the range [2.9:3.1] g cm^{-3}, close to the conditions of the present study, the in-plane thermal conductivity of non-hydrogenated a-SiN is equal to 2.5 to 3.7 W K^{-1} m^{-1} for film thicknesses between 50 nm and 4 μm [11, 39–41]. Although the thermal conductivity obtained in our calculations increases between 1.5 and 8 nm, it remains smaller than the values quoted above for the bulk.

IV. DISCUSSION

Thermal conductivity obtained through molecular dynamics methodologies has been shown to be size dependent, different theoretical frameworks leading to (slightly) different definition of the relevant quantities, such as the relevant cell dimension in the propagation direction. This issue has been thoroughly addressed in Ref. [42]. Within the AEMD approach, the increase of thermal conductivity κ with the period L of the temperature profile has been previously rationalized [31, 33, 43, 44]

ACCEPTED MANUSCRIPT
The Journal of Chemical Physics
AIP Publishing
This is the author's peer reviewed, accepted manuscript. However, the online version of record will be different from this version once it has been copyedited and typeset.
PLEASE CITE THIS ARTICLE AS DOI: 10.1063/5.0193566

by invoking non-local effects expected to arise at short lengths [45], namely when L is smaller than the maximum value of the phonon mean free paths (MaxMFP) distribution. Heat carriers experiencing a scattering event for distances larger than the cell dimension (in the direction of the transport) follow a ballistic regime, leading to a reduction of the thermal conductivity. Indeed, this same trend is observed in thermal transient grating experiments [46–48]. The coexistence of ballistic and diffusive propagation has been modeled by Alvarez and Jou [49] through the following expression:

$$\kappa_{\mathrm{AJ}}(L) = \kappa_{\mathrm{bulk}} \frac{L^2}{2\pi^2 l^2} \left[\sqrt{1 + 4 \left(\frac{\pi l}{L} \right)^2} - 1 \right], \quad (2)$$

where κ_{bulk} is the bulk thermal conductivity and l is an average value of the mean free path distribution. The success of Eq. 2 in fitting the AEMD results has been first demonstrated in the case of crystalline silicon [33]. More recently, we have been able to show that Eq. 2 works very well also for amorphous materials [50–52].

In Fig. 7 we present the results obtained for $\kappa(L)$ upon applying the AEMD strategy to several amorphous materials belonging either to the chalcogenide or to the dielectric insulators families. In the case of $Ge_2Sb_2Te_5$

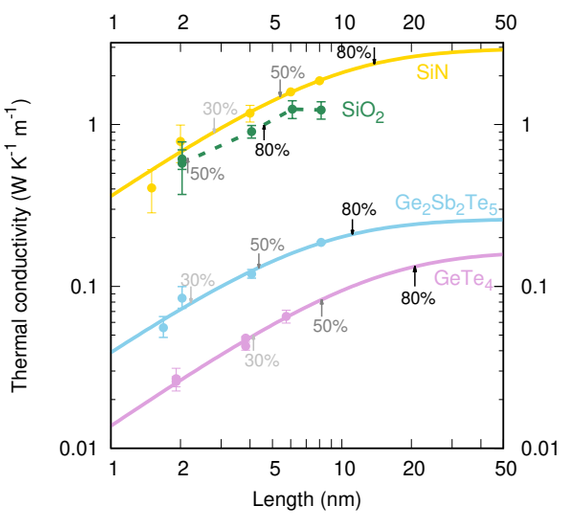

FIG. 7. Thermal conductivity of amorphous SiN, SiO_2, $Ge_2Sb_2Te_5$ and $GeTe_4$ versus the length of the periodic signal. The dots refer to the AEMD averaged results plotted with their error bars. The continuous curves are fits to Eq. 2. The dashed green line is just a guide for the eye. The grey arrows indicate the length corresponding to a thermal conductivity equal to 80, 50 or 30% of the bulk value.

[52] and $GeTe_4$ [32, 50, 51, 53], the increase of the thermal conductivity is rather similar to the trend observed here for a-SiN. For the three materials, Eq. 2 follows remarkably well the AEMD results, with the parameters reported in Tab. III.

As a valuable byproduct, Eq. 2 can be extrapolated to the bulk thermal conductivity regardless of any saturation in the trend exhibited by $\kappa(L)$, thereby allowing for an effective comparison between κ_{bulk} and reported measurements. For a-SiN, we obtain $\kappa_{\mathrm{bulk}} = 2.96 \pm 0.58$ W K^{-1} m^{-1} to be compared with the range of available measured data (2.5 to 3.7 W K^{-1} m^{-1}). We notice that the thermal conductivity of our largest system containing 1360 atoms amounts to 63 % of the bulk value. In view of the overall quality of the fit, showing optimal consistency between Eq. 2 and our FPMD data, this makes the extrapolation to larger (bulk) sizes particularly trustworthy. The excellent agreement recorded substantiates previous evidence collected for amorphous SiO_2, $Ge_2Sb_2Te_5$ and $GeTe_4$ by confirming the ability of AEMD to predict the behavior of thermal conductivity quantitatively. We stress that in the case of amorphous SiO_2 the agreement between the values of κ found for the largest sizes considered and the experimental bulk counterpart did not require any extrapolation [54].

In view of the available theories for heat transport in amorphous materials, highlighting somewhat differing views of the underlying mechanism [4, 5, 55, 56], it is worth recalling that the AEMD is devoid of any phenomenological assumption, relying on two main quantitative ingredients. First, the production of temporal trajectories at finite temperature via statistical mechanics, with forces obtained, in the present case, from a robust theoretical framework accounting for chemical bonding (density functional theory within FPMD). Second, the atomic-scale determination of the decay time τ leading to the thermal conductivity via Eq. 1. Based on the validity of the results obtained so far in comparison with experiments, we do consider AEMD as a theoretical tool of unprecedented predictive power.

The question arises on whether or not the results obtained by AEMD do agree with theories on the underlying heat conduction mechanism in amorphous materials. The Allen-Feldman model [57] was developed to describe the diffuson contribution, in addition to the Boltzmann transport equation for the propagative one. Recently, the quasi-harmonic Green-Kubo (QHGK) [56] and the Wigner transport equation (WTE) [4, 5] approaches succeeded in unifying the description of the two contributions into one formalism. In amorphous silica [5], the propagative contribution obtained with these models was found negligible, which could be reconciled with the AEMD observation that the thermal conductivity of silica saturates at very short lengths. This undermines any assumption on a phonon-like mode of propagation. In the amorphous Ge-based GeTe [58], $GeTe_4$ and $Ge_2Sb_2Te_5$ [59] on the other hand, the above models concur with a negligible contribution of the heat propagation, in favor of a diffuson-based process. This last result is in contrast with the length dependence of the thermal conductivity observed by AEMD for amorphous $GeTe_4$, $Ge_2Sb_2Te_5$ and SiN, which extends to hundreds of nanometers and is more in favor of propagation, since it closely follows

ACCEPTED MANUSCRIPT
The Journal of Chemical Physics
AIP Publishing
This is the author's peer reviewed, accepted manuscript. However, the online version of record will be different from this version once it has been copyedited and typeset.
PLEASE CITE THIS ARTICLE AS DOI: 10.1063/5.0193566

	a-SiN	a-SiO_2	a-GST	a-$GeTe_4$
κ_{bulk} (W K^{-1} m^{-1})	2.96±0.58	1.24±0.01	0.26±0.04	0.17±0.06
l(nm)	2.45±0.74	–	1.97±0.53	3.68±1.77
L(nm)@80%	14	5	11	21
L(nm)@50%	5	2	4	8
L(nm)@30%	3	–	2	4

TABLE III. Bulk thermal conductivities (κ_{bulk}) at saturation (a-SiO_2) and from the fit to Eq. 2 (for the 3 other amorphous models). The average mean free path (l) obtained from the fit is given for the latest. The lengths L corresponding to a thermal conductivity equal to 80, 50 and 30% of κ_{bulk} are also reported.

Eq. 2, which was derived assuming propagative heat transport. In this context, it is worth underlying that extrapolating $\kappa(L)$ with Eq. 2 at macroscopic sizes in the case of amorphous SiN, $Ge_2Sb_2Te_5$ and $GeTe_4$ reflects the existence of a MaxMFP for the propagative modes extending beyond the size affordable by FPMD, i.e. tens of nanometers.

Overall, the importance of our results goes beyond the agreement found with the bulk limit of κ (either extrapolated or attained for the largest size considered) and the considerations developed on the nature of heat transport in amorphous materials. Indeed, our findings are indicative of the impact of downscaling on the thermal conductivity, as illustrated in Fig. 7 where a mean free path distribution limited to values of L below 5 nm has the consequence of reducing by a factor of 2 the thermal conductivity of a-SiN. Table III generalizes this analysis for the four amorphous materials, by focusing on the values of L when a reduction of thermal conductivity of 80, 50 or 30 % of the bulk value κ_{bulk} is observed. We can infer that, when allowing for MaxMFP values up to 5 nm in a-SiN, the thermal conductivity becomes very close to the one of bulk a-SiO_2 (1.2 W K^{-1} m^{-1}), in a way appealing from the standpoint of the miniaturization of electron devices.

V. CONCLUSION

The thermal conductivity of amorphous SiN has been obtained via first-principles molecular dynamics by implementing a transient thermal regime within the AEMD methodology. The procedure is applied to five models differing by their dimension L in the heat transport direction. Thermodynamic conditions leading to the production of an amorphous state have been obtained by setting up independent thermal cycles. The thermal conductivity increases with L, but it remains smaller than the experimental bulk value even for the largest model with $L = 8$ nm containing more than 1300 atoms. This difference is ascribed to the existence of propagative modes with a distribution of mean free paths extending above 8 nm. Such a behavior has already been observed in two amorphous chalcogenides, whereas a saturation was observed above 6 nm in amorphous silica. Finally, it occurs that, in a-SiN, a reduction of the thermal conductivity to values close to those recorded in bulk silica can be obtained by discarding heat carriers beyond 4 nm.

ACKNOWLEDGMENTS

This work was funded by the French National Research Agency (ANR) through the Programme d'Investissement d'Avenir under contract ANR-11-LABX-0058_NIE, ANR-17-EURE-0024 and ANR-10-IDEX-0002-02. The authors would like to acknowledge the High Performance Computing Center of the University of Strasbourg for supporting this work by providing access to computing resources. Part of them were funded by the Equipex Equip@Meso project (Programme Investissements d'Avenir) and the CPER Alsacalcul/Big Data. Calculations on the larger systems were performed by using resources from GENCI (Grand Equipement National de Calcul Intensif) (Grant A0**0910296 and A0**0905071).

DATA AVAILABILITY

The data that support the findings of this study are available from the corresponding author upon reasonable request.

[1] M. Le Gallo and A. Sebastian, An overview of phase-change memory device physics, Journal of Physics D: Applied Physics **53**, 213002 (2020).
[2] S. Cueff, A. Taute, A. Bourgade, J. Lumeau, S. Monfray, Q. Song, P. Genevet, B. Devif, X. Letartre, and L. Berguiga, Reconfigurable flat optics with programmable reflection amplitude using lithography-free phase-change material ultra-thin films, Advanced Optical Materials **9**, 2001291 (2021).
[3] J. Zhang, Y. Li, Z. Chen, Q. Liu, Q. Chen, and M. Chen, Amorphous electrode: From synthesis to electrochemical energy storage, Energy & Environmental Materials **6**, e12573 (2022).

ACCEPTED MANUSCRIPT
The Journal of Chemical Physics
AIP Publishing
This is the author's peer reviewed, accepted manuscript. However, the online version of record will be different from this version once it has been copyedited and typeset.
PLEASE CITE THIS ARTICLE AS DOI: 10.1063/5.0193566

[4] M. Simoncelli, N. Marzari, and F. Mauri, Unified theory of thermal transport in crystals and glasses, Nature Physics **15**, 809 (2019).
[5] M. Simoncelli, F. Mauri, and N. Marzari, Thermal conductivity of glasses: first-principles theory and applications, npj Computational Materials **9**, 106 (2023).
[6] Y. Liu, H. Liang, L. Yang, G. Yang, H. Yang, S. Song, Z. Mei, G. Csányi, and B. Cao, Unraveling thermal transport correlated with atomistic structures in amorphous gallium oxide via machine learning combined with experiments, Advanced Materials **35**, 2210873 (2023).
[7] Z. Zhang, Y. Guo, M. Bescond, J. Chen, M. Nomura, and S. Volz, How coherence is governing diffuson heat transfer in amorphous solids, npj Computational Materials **8**, 96 (2022).
[8] E. Lampin, P. L. Palla, P.-A. Francioso, and F. Cleri, Thermal conductivity from approach-to-equilibrium molecular dynamics, Journal of Applied Physics **114**, 033525 (2013).
[9] C. Massobrio, *The Structure of Amorphous Materials using Molecular Dynamics*, 2053-2563 (IOP Publishing, 2022).
[10] F. L. Riley, Silicon nitride and related materials, Journal of the American Ceramic Society **83**, 245 (2000).
[11] H. Ftouni, C. Blanc, D. Tainoff, A. D. Fefferman, M. Defoort, K. J. Lulla, J. Richard, E. Collin, and O. Bourgeois, Thermal conductivity of silicon nitride membranes is not sensitive to stress, Physical Review B **92**, 125439 (2015).
[12] A. Lambrecht, C. Massobrio, M. Boero, G. Ori, and E. Martin, Atomic structure of amorphous SiN: Combining Car-Parrinello and Born-Oppenheimer first-principles molecular dynamics, Computational Materials Science **211**, 111555 (2022).
[13] L. E. Hintzsche, C. M. Fang, T. Watts, M. Marsman, G. Jordan, M. W. P. E. Lamers, A. W. Weeber, and G. Kresse, Density functional theory study of the structural and electronic properties of amorphous silicon nitrides: Si_3N_{4-x}:H, Physical Review B **86**, 235204 (2012).
[14] R. Car and M. Parrinello, Unified Approach for Molecular Dynamics and Density-Functional Theory, Physical Review Letters **55**, 2471 (1985).
[15] M. Born and R. Oppenheimer, Annaler der Physik **IV. Folge**, 457 (1927).
[16] A. D. Becke, Density-functional exchange-energy approximation with correct asymptotic behavior, Physical Review A **38**, 3098 (1988).
[17] C. Lee, W. Yang, and R. G. Parr, Development of the Colle-Salvetti correlation-energy formula into a functional of the electron density, Physical Review B **37**, 785 (1988).
[18] N. Troullier and J. L. Martins, Efficient pseudopotentials for plane-wave calculations, Physical Review B **43**, 1993 (1991).
[19] S. Nosé, A molecular dynamics method for simulations in the canonical ensemble, Molecular Physics **52**, 255 (1984).
[20] S. Nosé, A unified formulation of the constant temperature molecular dynamics methods, The Journal of Chemical Physics **81**, 511 (1984).
[21] W. G. Hoover, Canonical dynamics: Equilibrium phase-space distributions, Physical Review A **31**, 1695 (1985).
[22] C. Massobrio, I. A. Essomba, M. Boero, C. Diarra, M. Guerboub, K. Ishisone, A. Lambrecht, E. Martin, I. Morrot-Woisard, G. Ori, C. Tugène, and S. D. Wansi Wendji, On the actual difference between the Nosé and the Nosé-Hoover thermostats: A critical review of canonical temperature control by molecular dynamics, Physica Status Solidi (b) **261**, 2300209 (2023).
[23] G. J. Martyna, M. L. Klein, and M. Tuckerman, Nosé–Hoover chains: The canonical ensemble via continuous dynamics, The Journal of Chemical Physics **97**, 2635 (1992).
[24] P. E. Blöchl and M. Parrinello, Adiabaticity in first-principles molecular dynamics, Physical Review B **45**, 9413 (1992).
[25] *CPMD-code: CPMD Copyright 1990-2022 by IBM Corp. and 1994-2001 by Max Planck Institute, Stuttgart. https://github.com/CPMD-code*.
[26] S. Le Roux, A. Bouzid, M. Boero, and C. Massobrio, Structural properties of glassy Ge_2Se_3 from first-principles molecular dynamics, Phys. Rev. B **86**, 224201 (2012).
[27] A. Bouzid, S. Le Roux, G. Ori, M. Boero, and C. Massobrio, Origin of structural analogies and differences between the atomic structures of $GeSe_4$ and GeS_4 glasses: A first principles study, The Journal of Chemical Physics **143**, 034504 (2015).
[28] S. Le Roux, A. Bouzid, M. Boero, and C. Massobrio, The structure of liquid GeSe revisited: A first principles molecular dynamics study, The Journal of Chemical Physics **138**, 174505 (2013).
[29] J. Hutter, Car-Parrinello molecular dynamics, WIREs Computational Molecular Science **2**, 604 (2012).
[30] D. Marx and J. Hutter, *Ab Initio Molecular Dynamics: Basic Theory and Advanced Methods* (Cambridge University Press, 2009).
[31] H. Zaoui, P. L. Palla, F. Cleri, and E. Lampin, Length dependence of thermal conductivity by approach-to-equilibrium molecular dynamics, Physical Review B **94**, 054304 (2016).
[32] A. Bouzid, H. Zaoui, P. L. Palla, G. Ori, M. Boero, C. Massobrio, F. Cleri, and E. Lampin, Thermal conductivity of glassy $GeTe_4$ by first-principles molecular dynamics, Physical Chemistry Chemical Physics **19**, 9729 (2017).
[33] P. L. Palla, S. Zampa, E. Martin, and F. Cleri, Interface thermal behavior in nanomaterials by thermal grating relaxation, International Journal of Heat and Mass Transfer **131**, 932 (2019).
[34] C. Melis, R. Dettori, S. Vandermeulen, and L. Colombo, Calculating thermal conductivity in a transient conduction regime: Theory and implementation, The European Physical Journal B **87**, 96 (2014).
[35] L. Yang and B.-Y. Cao, Significant anharmonicity of thermal transport in amorphous silica at high temperature, Physica Status Solidi (RRL) - Rapid Research Letters **16**, 2200217 (2022).
[36] H. Zhang, X. Gu, Z. Fan, and H. Bao, Vibrational anharmonicity results in decreased thermal conductivity of amorphous HfO_2 at high temperature, Phys. Rev. B **108**, 045422 (2023).
[37] N. Marzari, A. A. Mostofi, J. R. Yates, I. Souza, and D. Vanderbilt, Maximally localized wannier functions: Theory and applications, Rev. Mod. Phys. **84**, 1419 (2012).
[38] J. L. Braun, S. W. King, E. R. Hoglund, M. A. Gharacheh, E. A. Scott, A. Giri, J. A. Tomko, J. T. Gaskins, A. Al-kukhun, G. Bhattarai, M. M. Paquette,

ACCEPTED MANUSCRIPT
The Journal of Chemical Physics
AIP Publishing
This is the author's peer reviewed, accepted manuscript. However, the online version of record will be different from this version once it has been copyedited and typeset.
PLEASE CITE THIS ARTICLE AS DOI: 10.1063/5.0193566

G. Chollon, B. Willey, G. A. Antonelli, D. W. Gidley, J. Hwang, J. M. Howe, and P. E. Hopkins, Hydrogen effects on the thermal conductivity of delocalized vibrational modes in amorphous silicon nitride ($a-SiN_x$:H), Phys. Rev. Mater. **5**, 035604 (2021).

[39] C. H. Mastrangelo, Y.-C. Tai, and R. S. Muller, Thermophysical properties of low-residual stress, silicon-rich, LPCVD silicon nitride films, Sensors and Actuators A: Physical **23**, 856 (1990), Proceedings of the 5th International Conference on Solid-State Sensors and Actuators and Eurosensors III.

[40] B. Zink and F. Hellman, Specific heat and thermal conductivity of low-stress amorphous SiN membranes, Solid State Communications **129**, 199 (2004).

[41] M. T. Alam, M. P. Manoharan, M. A. Haque, C. Muratore, and A. Voevodin, Influence of strain on thermal conductivity of silicon nitride thin films, Journal of Micromechanics and Microengineering **22**, 045001 (2012).

[42] Y. Sheng, Y. Hu, Z. Fan, and H. Bao, Size effect and transient phonon transport mechanism in approach-to-equilibrium molecular dynamics simulations, Phys. Rev. B **105**, 075301 (2022).

[43] H. Zaoui, P. L. Palla, F. Cleri, and E. Lampin, Fourier-like conduction and finite one-dimensional thermal conductivity in long silicon nanowires by approach-to-equilibrium molecular dynamics, Physical Review B **95**, 104309 (2017).

[44] H. Zaoui, P. L. Palla, S. Giordano, F. Cleri, M. Verdier, D. Lacroix, J.-F. Robillard, K. Termentzidis, and E. Martin, Thermal conductivity of deca-nanometric patterned Si membranes by multiscale simulations, International Journal of Heat and Mass Transfer **126**, 830 (2018).

[45] G. D. Mahan and F. Claro, Nonlocal theory of thermal conductivity, Physical Review B **38**, 1963 (1988).

[46] A. J. Minnich, Determining Phonon Mean Free Paths from Observations of Quasiballistic Thermal Transport, Physical Review Letters **109**, 205901 (2012).

[47] J. Cuffe, J. K. Eliason, A. A. Maznev, K. C. Collins, J. A. Johnson, A. Shchepetov, M. Prunnila, J. Ahopelto, C. M. Sotomayor Torres, G. Chen, and K. A. Nelson, Reconstructing phonon mean-free-path contributions to thermal conductivity using nanoscale membranes, Physical Review B **91**, 245423 (2015).

[48] T. Kim, J. Moon, and A. J. Minnich, Origin of micrometer-scale propagation lengths of heat-carrying acoustic excitations in amorphous silicon, Physical Review Materials **5**, 065602 (2021).

[49] F. X. Alvarez and D. Jou, Memory and nonlocal effects in heat transport: From diffusive to ballistic regimes, Applied Physics Letters **90**, 083109 (2007).

[50] T.-Q. Duong, C. Massobrio, G. Ori, M. Boero, and E. Martin, Thermal conductivity and transport modes in glassy $GeTe_4$ by first-principles molecular dynamics, Physical Review Materials **3**, 105401 (2019).

[51] T.-Q. Duong, C. Massobrio, M. Boero, G. Ori, and E. Martin, Heat transport in disordered network forming materials: Size effects and existence of propagative modes, Computational Materials Science **177**, 109607 (2020).

[52] T.-Q. Duong, A. Bouzid, C. Massobrio, G. Ori, M. Boero, and E. Martin, First-principles thermal transport in amorphous $Ge_2Sb_2Te_5$ at the nanoscale, RSC Advances **11**, 10747 (2021).

[53] E. Martin, P. L. Palla, F. Cleri, A. Bouzid, G. Ori, S. Le Roux, M. Boero, and C. Massobrio, On the occurrence of size effects in the calculation of thermal conductivity by first-principles molecular dynamics: The case of glassy $GeTe_4$, Journal of Non-Crystalline Solids **498**, 190 (2018).

[54] E. Martin, G. Ori, T.-Q. Duong, M. Boero, and C. Massobrio, Thermal conductivity of amorphous SiO_2 by first-principles molecular dynamics, Journal of Non-Crystalline Solids **581**, 121434 (2022).

[55] P. B. Allen, J. L. Feldman, J. Fabian, and F. Wooten, Diffusons, locons and propagons: Character of atomic vibrations in amorphous Si, Philosophical Magazine B **79**, 1715 (1999).

[56] L. Isaeva, G. Barbalinardo, D. Donadio, and S. Baroni, Modeling heat transport in crystals and glasses from a unified lattice-dynamical approach, Nature Communications **10**, 3853 (2019).

[57] P. B. Allen and J. L. Feldman, Thermal conductivity of disordered harmonic solids, Phys. Rev. B **48**, 12581 (1993).

[58] G. C. Sosso, D. Donadio, S. Caravati, J. Behler, and M. Bernasconi, Thermal transport in phase-change materials from atomistic simulations, Physical Review B **86**, 104301 (2012).

[59] L. Yang and B.-Y. Cao, Thermal transport of amorphous phase change memory materials using population-coherence theory: a first-principles study, Journal of Physics D: Applied Physics **54**, 505302 (2021).